Optimal Electron Doping of a C_{60} Monolayer on Cu(111) via Interface Reconstruction

Woei Wu Pai,[1,*] H. T. Jeng,[2,3,†] C.-M. Cheng,[4] C.-H. Lin,[1] Xudong Xiao,[5] Aidi Zhao,[5] Xieqiu Zhang,[5] Geng Xu,[6,§] X. Q. Shi,[6] M. A. Van Hove,[6] C.-S. Hsue,[3] and K.-D. Tsuei[3,4,‡]

[1]*Center for Condensed Matter Sciences, National Taiwan University, Taipei 106, Taiwan*
[2]*Institute of Physics, Academia Sinica, Taipei 115, Taiwan*
[3]*Department of Physics, National Tsing Hua University, Hsinchu 300, Taiwan*
[4]*National Synchrotron Radiation Research Center, Hsinchu 300, Taiwan*
[5]*Department of Physics, Hong Kong University of Science and Technology, Clear Water Bay, Hong Kong*
[6]*Department of Physics, City University of Hong Kong, Kowloon, Hong Kong*

(Received 6 September 2009; published 22 January 2010)

We demonstrate the charge state of C_{60} on a Cu(111) surface can be made optimal, i.e., forming $C_{60}{}^{3-}$ as required for superconductivity in bulk alkali-doped C_{60}, purely through interface reconstruction rather than with foreign dopants. We link the origin of the $C_{60}{}^{3-}$ charge state to a reconstructed interface with ordered (4×4) 7-atom vacancy holes in the surface. In contrast, C_{60} adsorbed on unreconstructed Cu(111) receives a much smaller amount of electrons. Our results illustrate a definitive interface effect that affects the electronic properties of molecule-electrode contact.

DOI: 10.1103/PhysRevLett.104.036103 PACS numbers: 68.43.−h, 61.05.jh, 68.35.Ct, 73.20.−r

In bulk fulleride A_nC_{60} (A = Na, K, etc.) [1], an "optimal doping" state favoring superconductivity is known to occur for $n = 3$, with 3 electrons on each C_{60} ($C_{60}{}^{3-}$). Since C_{60} films on metallic surfaces typically involve substrate-to-C_{60} electron transfer that partially populates the C_{60} lowest unoccupied molecular orbital (LUMO), it has been of great interest to pursue optimally doped C_{60} films. Earlier studies show that the electron transfer amount does not simply depend on the substrate work function [2]. This raises the question of the role of the C_{60}/metal interface structure. Although strong C_{60}-metal interactions are not expected for, e.g., C_{60} on noble metal surfaces, there is increasing evidence of C_{60}-induced interface reconstruction for C_{60}/Au(110) [3], C_{60}/Pt(111) [4], C_{60}/Al(111) [5], C_{60}/Ag(100) [6], and even for C_{60}/Ag(111) [7] and C_{60}/Cu(111) [8], etc. The typical scenario is that C_{60} tends to dig a "vacancy" in the surface. Calculations, including our own, show this geometry increases the adsorption strength that compensates the energy cost of vacancy creation. No studies, however, have discussed how the electronic structure and hence the charge state of a C_{60} film are affected by its interface structure. Here, we discovered that a C_{60} monolayer on Cu(111) is optimally electron doped purely by interface reconstruction and without intercalating alkali atoms. We convincingly establish the $C_{60}{}^{3-}$ charge state and trace its origin to a reconstructed interface with ordered (4×4) large 7-atom vacancy holes in the surface. The key link between molecular doping and a reconstructed interface indicates the practical needs of tackling the often neglected difficult interface structure problems which could prove essential in understanding the physics and chemistry of thin film materials.

Many inconsistencies between experiment and theory in heteroepitaxial systems, such as the charge state of a C_{60} film on a surface, are likely rooted in the application of an incorrect interface model. For C_{60}/Cu(111), it has been measured to range from 1–3 electrons per C_{60} by photoemission spectroscopy (PES) [9]. Calculations predict a much smaller amount, $<0.8e^-$, for an unreconstructed interface [10]. The electronic band structure measured by a recent PES study is also at odds with theoretical analysis under the same assumption [11]. These conflicts are resolved by our ordered (4×4) 7-atom vacancy interface model. Because the structure can be alternatively viewed as having 9 Cu adatoms per unit cell at C_{60} exohedral sites, the C_{60} molecules can also be understood as doped by Cu adatoms.

The substrate-to-C_{60} electron transfer have been roughly estimated from the softening of C_{60} vibration modes [12], LUMO peak intensity in PES, etc. The most precise measurement would be a complete band mapping from angle-resolved (AR)PES. We have thus prepared well-ordered monolayer C_{60} films and mapped the bands at 30 K. The C_{60} film was obtained by depositing excess C_{60}, followed by annealing at 570 K to eliminate C_{60} multilayers. The PES spectra were taken at U9-CGM (NSRRC, Taiwan) with a Scienta SES-200 hemispherical analyzer with a collecting angle of ±8°, a photon energy of 31.5 eV for AIPES and 22 eV for ARPES, and an overall energy resolution of 12 meV. Figure 1(a) depicts the Fermi surface (FS) with a ±20 meV energy integration window. At least two regions of FS crossing were observed around the $\bar{\Gamma}$ and $\bar{K}$ points. Figure 1(b) shows the band dispersion along $\bar{\Gamma}$-$\bar{M}$ and $\bar{\Gamma}$-$\bar{K}$. There is an occupied state around $\bar{\Gamma}$, generating an electronlike FS. Another FS crossing occurs near $\bar{K}$ and is attributed to holelike band dispersion. In Fig. 1(c), this holelike band dispersion is manifested in the measured momentum distribution curves (MDC). There are actually two FS crossings near $\bar{K}$ along $\bar{\Gamma}$-$\bar{K}$-$\bar{M}$ at $k_{\parallel} \sim 0.27$ Å^{-1}

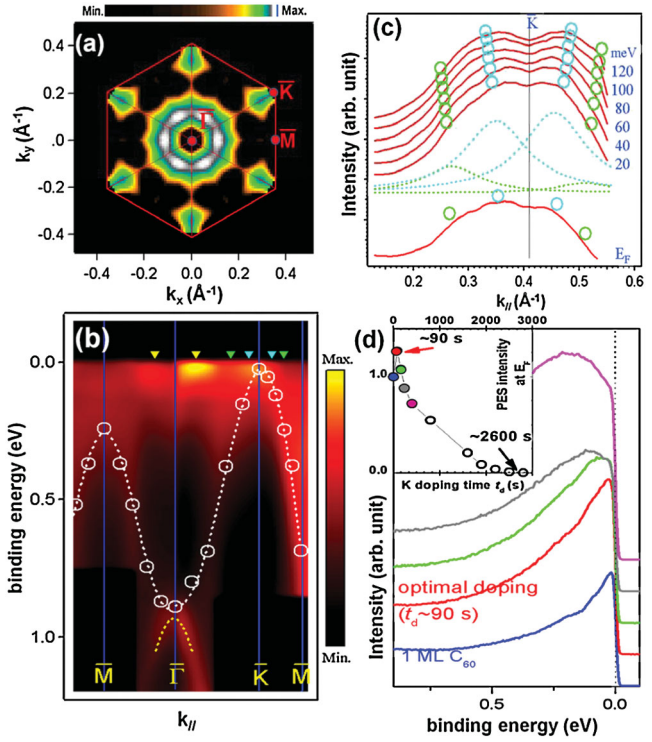

FIG. 1 (color). (a) Fermi surface (FS) mapping of 1 ML C_{60}. At least two regions of FS crossings were observed around $\bar{\Gamma}$ and $\bar{K}$. (b) Band dispersion along $\bar{\Gamma}$-$\bar{M}$ and $\bar{\Gamma}$-$\bar{K}$. FS crossings are marked by three pairs of colored triangles. The white circles denote the calculated LUMO-derived bands and the white dashed line is a guide to the eyes. The size of the circles indicates the accuracy of the extracted band position. (c) Measured MDC near the $\bar{K}$ point at various binding energies. The circles are the fitted positions of the two holelike dispersive bands. (d) AIPES spectra vs doping time (t_d) for the first five studied t_d. As K atoms are doped, the LUMO peak shifts to higher binding energy. The inset shows the LUMO intensity at E_F vs t_d.

and 0.35 Å^{-1} (also at 0.52 Å^{-1} and 0.46 Å^{-1}), as denoted by the green and the blue circles. The circles are fitted Lorentzian peak positions of the holelike band dispersion near the FS crossings. The amount of electron transfer is calculated by the Luttinger volume of the occupied FS area [13]. Assuming circular bands crossing near $\bar{\Gamma}$ and $\bar{K}$, there are ~0.09 electrons for the electron pocket around $\bar{\Gamma}$ and ~1.09 plus ~1.82 electrons for the two holelike bands near $\bar{K}$ per unit cell. The total amount of electron transfer from Cu is thus ~3 electrons per C_{60}. This renders the C_{60} LUMO half-filled, and the C_{60} film is therefore nearly "optimally doped." We also verified this extraordinary electron transfer using angle-integrated (AI)PES. The AIPES LUMO intensity at the Fermi energy (E_F) was tracked as potassium (K) atoms evaporated from a calibrated SAES getter source were incorporated into a C_{60} monolayer. The optimally doped ("K_3C_{60}, C_{60}^{3-}") and fully doped ("K_6C_{60}, C_{60}^{6-}") states have maximum and zero LUMO intensity at E_F, respectively [14,15]. Figure 1(d) depicts the evolution of AIPES spectra with K doping, and its inset shows the spectra intensity at E_F vs K doping time. We note that the "K_3C_{60}" state was achieved with very slight K doping (~90 s of dose time). Since "K_6C_{60}" was obtained after ~2600 s of dose time, a linear extrapolation shows that only ~0.1 K atom per C_{60} is required to render the 1 ML C_{60} film optimally doped. Consequently, each C_{60} already accepts ~2.9e^- from the Cu(111) substrate, consistent with the ARPES result.

Various electron transfer values for C_{60} on Cu(111) have been reported in experiments [9,11,12]. Here, we confirm the extraordinary ~3e^- charge transfer, being the largest value reported for undoped C_{60} monolayers. By using scanning tunneling microscopy and spectroscopy (STM/STS), we show that this charge transfer is related to interface reconstruction. STM and STS were conducted with a commercial Omicron variable-temperature microscope and a low-temperature microscope housed in two chambers with a base pressure $<4 \times 10^{-11}$ Torr. In our previous studies [8,16], we prepared "core-shell" islands with a two-stage method by first depositing C_{60} at ~500 K (for the "core" with a reconstructed interface) and then C_{60} at ~250 K (for the "shell" with an unreconstructed interface). A typical core-shell C_{60} island is shown in Fig. 2(a). STS spectra taken at 77 K showed that the LUMO peak in the shell region was located ~0.75 V above E_F [dashed line, Fig. 2(b)], indicating a minor charge transfer. If the LUMO peak is approximately symmetric and has a peak position at E_F, the band can be viewed as half-filled. In the core region, the LUMO peak shifts to a position slightly above E_F (solid line). This suggests that nearly ~3e^- are transferred to each C_{60}, consistent with the PES results.

Strong chemical bonding between C_{60} and Cu(111) must have occurred to facilitate the observed large charge transfer. In order to investigate the bonding, we studied the interface structure in details. In Fig. 2(a), the STM topographic height of the core region is ~2 Å lower than

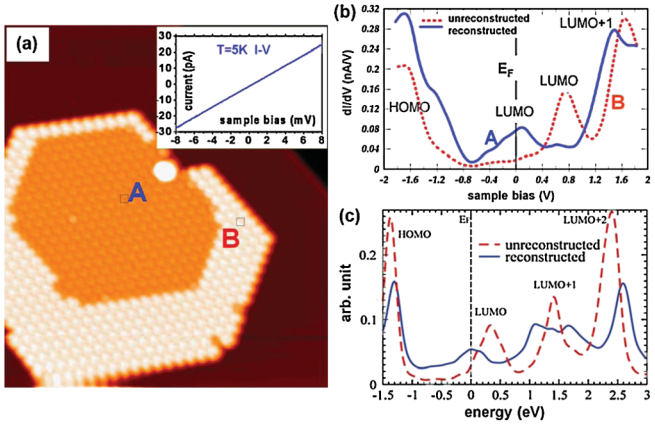

FIG. 2 (color). (a) A "core-shell" island (35 nm × 35 nm). (b) STS spectra show a dramatic shift of the LUMO band in the reconstructed core vs unreconstructed shell region. $T = 77$ K. (c) Calculated C_{60} PDOS of the unreconstructed and reconstructed (r-fcc) C_{60}/Cu(111) with 0.1 eV Gaussian broadening. The inset of (a) shows no energy gap near E_F in STS at ~5 K.

that of the shell region [8]. This large height difference suggests that the interface must have enough missing atoms to let a C_{60} "sink" by ~2 Å [17]. The number of missing Cu atoms, N, in a (4×4) unit cell can be obtained from a mass-flow analysis by *in situ* STM monitoring of C_{60} growth. This number is critical because it allows us to readily rule out implausible models. Our conclusion is that $N \sim 7.1 \pm 0.7$ [17], thus leaving 9 out of $4 \times 4 = 16$ atoms per unit cell if the 7 atoms are removed from the outermost Cu layer.

A straightforward reconstructed interface model with a top layer Cu atom density of 9/16 is an ordered nanotemplate of 7-atom monolayer holes [Fig. 3(a)], in which strings of top layer Cu atoms are arranged in the kagome lattice. Previous experiments with STM [8,18] and x-ray photoelectron diffraction (XPD) [19] implied a C_{60} orientation with its hexagonal ring facing down and two coexisting high-symmetry azimuthal orientations differing by 60°. The combined substrate-C_{60} orientation is characterized by C_3 symmetry. The Fig. 3(a) model adopts this experimentally determined C_{60} orientation. Our *ab initio* calculations estimate that the reconstruction model is favored by ~0.2 eV/cell over the unreconstructed case [17]. In the Fig. 3(a) model, the C_{60} center can either sit at an fcc or an hcp site, depending on whether the top layer Cu atoms are stacked at unfaulted fcc or faulted hcp sites. Henceforth, we denote these two reconstructed cases as the r-fcc and r-hcp models. Our calculations give very similar energies for the two structures. There is a slight preference for hcp-site C_{60} adsorption (~0.01 eV/cell lower) if the slab used in the calculation is thinner than ~15 Cu layers. For thicker slabs (from 18 to 30 Cu layers), the r-fcc structure becomes ~0.02 eV/cell lower in energy. A large barrier, ~0.5 eV/cell, prevents a transition between the r-fcc and r-hcp structures. The azimuthal C_{60} rotation barrier is large, i.e., ~2 eV. When the interface is left unreconstructed, C_{60} preferably adsorbs at hcp sites by ~0.02 eV/cell, consistent with a previous calculation [10].

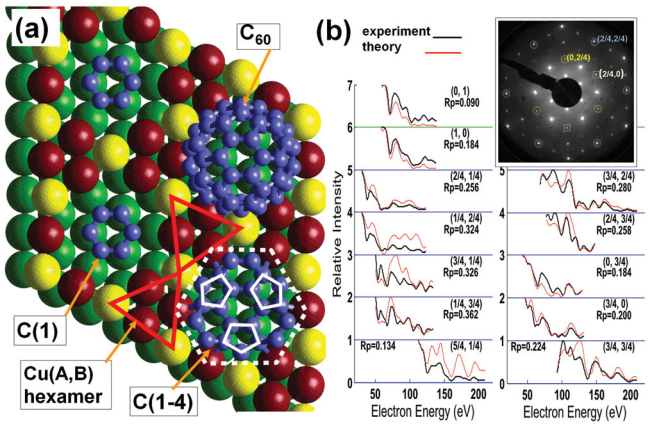

FIG. 3 (color). (a) The reconstructed model of the C_{60}/Cu(111) interface. Color scheme: First layer Cu(A) (red) and Cu(B) (yellow), second layer Cu (green), C atoms (blue). C(N), $N = 1, 2, \ldots$ denotes the bottom Nth C layer of a C_{60}. The C(1) layer, C(1-4) portion, and a full C_{60} are all depicted. The top Cu layer is significantly distorted, leading to alternating rotation of Cu(A, B) hexamers (red solid line) on a honeycomb sublattice and a distorted Cu(A) hexagon(white dashed line). (b) Selected LEED I-V beams and their tensor LEED fitting. Inset: a typical LEED pattern.

We performed an extensive tensor LEED I-V curve fitting to a very large experimental database for quantitative structure determination. Experimental I-V curves were extracted with code developed in-house. The LEED analysis was performed with our symmetrized automated tensor LEED code [17]. A total energy fitting range of ~3500 eV was used to evaluate the Pendry R factor. We used 33 independent beams taken at room temperature between 20 and 210 eV to fit 102 independent parameters. Initial test structures were based on fully relaxed theoretical coordinates. Test models with C_{60} orientations clearly inconsistent with the STM and XPD were excluded. Two mirror domains of azimuthal C_{60} orientation are mixed with equal weight because the experimental LEED pattern shows C_{3v} symmetry instead of the C_3 symmetry of a single C_{60} domain. We optimized both the (a) unreconstructed and the (b) reconstructed interface models. The best LEED Pendry R factors are (a) 0.330 versus (b) 0.572 before optimization. After optimization, we obtained (a) 0.324 versus (b) 0.274. The ~17% difference in R factors shows that interface reconstruction is clearly favored. Furthermore, we compared the faulted r-hcp model with the unfaulted r-fcc reconstructed model. Before optimization, the Pendry R factors are (r-hcp) 0.568 versus (r-fcc) 0.572. After optimization, we obtained (r-hcp) 0.304 versus (r-fcc) 0.274. The ~11% difference indicates that the r-fcc model is preferred. The single adsorption site of C_{60}, as determined here by LEED, was inferred previously from our STM study [8] but is at odds with an earlier STM result [18]. In C_{60}/Pt(111) [4] and C_{60}/Ag(111) [7], a C_{60} is found to reside atop a single atom vacancy, rather than a 7-atom vacancy. We also tested this unlikely single-vacancy model. The optimized R factor is 0.406 and is clearly unfavorable. Compared with a recently published LEED determination of C_{60}/Ag(111) [7] with an R factor of 0.36, our analysis yields an R factor of ~0.27. Figure 3(b) shows selected measured and fitted LEED I-V curves.

Our LEED analysis and *ab initio* results illustrate a salient structural feature: the strong Cu-C_{60} bonding is enhanced not only by pulling a C_{60} into a Cu "bowl," but also by significantly distorting the top Cu layer. In Fig. 3(a), there are several short C-Cu bonds. We denote the red Cu atoms as Cu(A), yellow Cu atoms as Cu(B), and the bottom Nth layer C atoms as C(N), where C(1) is the bottom C hexagon. The Cu(A)-C(2) bonds are the shortest, with an average bond length of 2.10 Å (theory) and 1.98 Å (LEED). The other strong Cu-C bonds are Cu(A)-C(4) and Cu(B)-C(3), with bond lengths of 2.40 and 2.31 Å, respectively (theory), and 2.30 Å and 2.14 Å (LEED). The bond lengths between the second layer Cu atoms (green) and the

closest bottom C(1) atoms are ~2.25 Å (theory) and ~2.20 Å (LEED). The consistent trend of shorter Cu-C bond lengths in the best-fit LEED model suggests that C_{60} is bonded closer to the Cu substrate than theory predicts. The various C and Cu(*A, B*) bond lengths result in alternating clockwise and counterclockwise Cu(*A, B*) hexamer (red solid line) rotation on a honeycomb sublattice and a distorted Cu(*A*) hexagon (white dashed line) that collaboratively enhance C_{60}-Cu bonding. To our knowledge, C_{60} is the first known intact molecule to cause extensive reconstruction of Cu(111). This special structural stability derives from an intricate matching of the Cu lattice spacing, the (4×4) ordering, the C_{60} orientation, and the top Cu layer distortion, and it is quite unique and remarkable.

Based on our interface model, we recalculated the partial density of states (PDOS) and band dispersion to compare with the STS and PES data. C_{60} PDOS curves for both the unreconstructed and reconstructed r-fcc models are shown in Fig. 2(c). The C_{60} molecular orbital band energies obtained for the unreconstructed case are similar to previous theoretical results [10] and the limited LUMO occupancy indicates an estimated electron transfer $<1e^-/C_{60}$. In the r-fcc model, the LUMO-derived band energy is lowered by 0.35 eV and is near the Fermi level and nearly half-filled, indicating a charge transfer of $\sim 3e^-/C_{60}$ in excellent agreement with PES and STS. Note that the overall band intensity suppression and band width broadening in the r-fcc model indicate strong C_{60} and Cu(111) interactions. The band dispersion was also analyzed theoretically [Fig. 1(b)]. The LUMO-derived bands were extracted by analyzing the carbon-projected electron density. The band maximum appears very near E_F at $\bar{K}$ and the bands lie well below E_F elsewhere in the surface Brillouin zone; both are in agreement with the experiments. The calculation is however unable to clearly distinguish two separate hole bands, unlike the MDC in Fig. 1(c). For the unreconstructed interface, such a holelike band is completely missing. Another state that disperses downward from $\bar{\Gamma}$ (yellow dotted line) was observed in ARPES [Fig. 1(b)]. This band was previously attributed to an anisotropic interface state [11]. Our calculations find it contains significant carbon contribution around $\bar{\Gamma}$.

In optimally alkali-doped bulk C_{60} fullerides, e.g., "K_3C_{60}," superconductivity has been observed [1]. We tested our alkali-free and optimally doped C_{60} monolayer for 2D surface superconductivity [20]. With STS, we found no sign of an energy gap down to ~5 K [Fig. 2(a) upper inset]. Likely, the ultrathin thickness [21] and the triangular symmetry of a C_{60} monolayer tend to prohibit Cooper pair formation. A surface superconductivity transition, if present, must have been suppressed to an even lower temperature. We expect our study to spawn further investigations of C_{60}/Cu(111) for 2D superconductivity.

Finally, it indeed takes a combination of techniques and theoretical analysis to unambiguously determine the C_{60}-substrate interface structure. Our calculated C_{60} STM images (not shown) vary only slightly with reconstruction. STS-PDOS, ARPES, and the total energy are all sensitive to reconstruction, but cannot clearly distinguish the r-fcc and r-hcp models. Ultimately, it is the LEED *I-V* analysis that confirms the r-fcc model. The 7-atom vacancy holes observed in C_{60}/Cu(111) interface are much larger than the single-vacancy holes previously observed [4,7]. We believe the more corrugated C_{60}/Cu(111) interface allows more intimate substrate-molecule contact and is likely the key of "adatom self doping" that renders C_{60} optimally doped. Our endeavor to elucidate doping-structure correlation at a molecular-substrate interface adds a new dimension in understanding functional molecular thin films.

This work was supported by NSC, NSRRC, NCHC, NCTS, NTU, Taiwan, and also in part by RGC Grant No. CityU1/02C, by CityU Grant No. 9380041, and by the CityU Centre for Applied Computing and Interactive Media. We thank Dr. C. M. Wei and Dr. G. M. Gavaza for fruitful discussions.

*Corresponding author.
wpai@ntu.edu.tw
†Corresponding author.
jeng@phys.sinica.edu.tw
‡Corresponding author.
tsuei@nsrrc.gov.tw
§Permanent address: Physics Department, ZhongShan(Sun Yat-Sen) Univ., Guangzhou, 510275, China.

[1] A. F. Hebard *et al.*, Nature (London) **350**, 600 (1991).
[2] C. T. Tzeng *et al.*, J. Phys. Condens. Matter **19**, 176009 (2007).
[3] M. Hinterstein *et al.*, Phys. Rev. B **77**, 153412 (2008).
[4] R. Felici *et al.*, Nature Mater. **4**, 688 (2005).
[5] M. Stengel, A. De Vita, and A. Baldereschi, Phys. Rev. Lett. **91**, 166101 (2003).
[6] W. W. Pai and C. L. Hsu, Phys. Rev. B **68**, 121403(R) (2003).
[7] H. I. Li *et al.*, Phys. Rev. Lett. **103**, 056101 (2009).
[8] W. W. Pai *et al.*, Phys. Rev. B **69**, 125405 (2004).
[9] K.-D. Tsuei *et al.*, Phys. Rev. B **56**, 15 412 (1997).
[10] L. L. Wang and H. P. Cheng, Phys. Rev. B **69**, 045404 (2004).
[11] A. Tamai *et al.*, Phys. Rev. B **77**, 075134 (2008).
[12] C. Silien, P. A. Thiry, and Y. Caudano, Surf. Sci. **558**, 174 (2004).
[13] J. M. Luttinger, Phys. Rev. **119**, 1153 (1960).
[14] C. Cepek *et al.*, Surf. Sci. **454–456**, 766 (2000).
[15] A. Tamai *et al.*, Phys. Rev. B **72**, 085421 (2005).
[16] W. W. Pai *et al.*, Appl. Surf. Sci. **241**, 194 (2005).
[17] See supplementary material at http://link.aps.org/supplemental/10.1103/PhysRevLett.104.036103 for details on calculations and STM mass flow analysis.
[18] T. Hashizume *et al.*, Phys. Rev. Lett. **71**, 2959 (1993).
[19] R. Fasel *et al.*, Phys. Rev. Lett. **76**, 4733 (1996).
[20] S. Y. Qin *et al.*, Science **324**, 1314 (2009).
[21] J. W. Wu, Physica (Amsterdam) **439C**, 101 (2006).